Electronic Supplementary Information (ESI)

Crystal-Facet Modulated Pathway of CO_2 Photoreduction on Bi_4NbO_8Cl Nanosheets Boosting Production of Value-Added Solar Fuels

Peiting Hao,[a] Haoqiang Chi,[a] Zhengdao Li,*[b] Xinxin Lu,*[c] Yong Yang,[d] Yongcai Zhang,[e] Zhigang Zou, [a,f] and Yong Zhou,* [a,f]

[a] School of Physics, Jiangsu Key Laboratory of Nanotechnology, Eco-materials and Renewable Energy Research Center (ERERC), National Laboratory of Solid State Microstructures, Collaborative Innovation Center of Advanced Microstructures, Nanjing University, Nanjing 210093, P. R. China. E-mail: zhouyong1999@nju.edu.cn

[b] Chemistry and Pharmaceutical Engineering College, Engineering Technology Research Center of Henan Province for Solar Catalysis, Nanyang Normal University, Nanyang, Henan 473061, P. R. China. E-mail: nylzd@nynu.edu.cn

[c] PetroChina Shenzhen New Energy Research Institute, Shenzhen, Guangdong, 518052, P. R. China. Email: lu.xinxin6391@gmail.com

[d] Key Laboratory of Soft Chemistry and Functional Materials (MOE), Nanjing University of Science and Technology, Nanjing, Jiangsu, 210094, P. R. China.

[e] School of Chemistry and Chemical Engineering, Yangzhou University, Yangzhou 225009, P. R. China.

[f] School of Science and Engineering, The Chinese University of Hongkong (Shenzhen), Shenzhen, Guangdong, 518172, P. R. China.

Experimental Section

All reagents used in the present study were analytical reagent grade. All chemicals were used as received. Deionized water was used throughout the synthesis.

Synthesis of Bi_4NbO_8Cl nanosheets: The Bi_4NbO_8Cl nanosheets exposed high-indexed (201) facets [designated as BNOC-(201)] were prepared by hydrothermal method. Firstly, 0.25 g Nb_2O_5, 1.685 g KOH and 30 mL deionized water were uniformly mixed in a hydrothermal reactor and heated to 180°C for 72 h. After natural cooling, the $[Nb_6O_{19}]^{8-}$ precursor solution was obtained. In the second step, 0.083 mmol $BiCl_3$, 0.92 mmol $Bi(NO_3)_3 \cdot 5H_2O$ and 0.40 g polyvinylpyrrolidone (PVP, K30) were dispersed in 20 mL 0.1 M mannitol solution, stirred for 30 min, 8.0 mL precursor solution was slowly added, and the pH was adjusted to 7.8 with HCl solution. The above solution was sealed in a hydrothermal reactor and heated to 260°C for 48 h. After cooling, the precipitate obtained by filtration was washed several times with deionized water and alcohol, and placed in a freeze dryer for freeze-drying for 72 h, BNOC-(201) were obtained. The synthesis of Bi_4NbO_8Cl nanosheets exposed (001) facets [designated as BNOC-(001)] is similar to the above, after adding the precursor solution, only a small amount of HCl solution needs to be added to adjust the pH to 8.5, and the following operations can be repeated.

Synthesis of Bulk Bi_4NbO_8Cl: The bulk phase Bi_4NbO_8Cl (designated as BNOC-B) was synthesized by high temperature calcination method. Firstly, 3.0 mmol Bi_2O_3 and 1.0 mmol Nb_2O_5 were mixed with 2.0 mmol BiOCl in agate mortar. Then, the above mixture was heated to 800°C in a muffle furnace and held for 4 h. After cooling to room temperature, the final yellow powder composed of dozens of microns of large microcrystals was obtained (Fig. S2, ESI†).

Photocatalytic CO_2 reduction: Photocatalytic reduction of CO_2 is a gas phase reaction. The reaction was carried out in a 170 mL stainless steel tank using a 300 W xenon lamp as the light source. 2 mg of the sample was evenly dispersed on a reactor with an area of about 4.2 cm^2, and 0.2 mL of deionized water was injected into the reaction system as a reducing agent. Before the irradiation, the reaction device was vacuum-treated several times, and then high-purity CO_2 gas (purity of 99.999%) was injected into the reaction device to reach 1.2 times the chamber pressure, and the temperature was raised to 180°C. During the photocatalytic reaction, about 5ml of gas was injected into the gas chromatograph (Agilent-8890, USA) from the reaction chamber every 1h to analyze the photocatalytic CO_2 reduction products of the material.

Characterizations: The crystallographic properties were determined by an X-ray diffractometer (Rigaku Ultimalll) with Cu Kα radiation (λ = 0.154178nm) at 40 kV and 40 mA with a scan rate of 5° min^{-1}. The microscopic morphology was investigated by scanning electron microscopy (Zeiss Gemini 500) coupled with energy-dispersive X-ray spectroscopy (Oxford Instruments Ultima Extreme). Atomic force microscopy (Asylum Research, MFP-3D-SA) was used to characterize the shape thickness of the sample. The surface contact potential difference (ΔCPD) was observed using a Kelvin probe force microscope (KPFM). Surface photovoltage microscopy (SPV) was detected using a light-assisted (405 nm laser excitation) KPFM. Ethanol is detected as a gaseous product. About 5ml of gas was sucked out with a specific needle and injected into the gas chromatograph (Agilent-8890, USA) from the reaction chamber every 1h to analyze.

Density functional theory (DFT) calculations

The spin-polarized DFT calculations were performed in the Vienna Ab-initio Simulation Package (VASP 6.1.0).[1, 2] The projector-augmented wave (PAW) approach[3, 4] and the Perdew-Burke-Ernzerhof (PBE) exchange-correlation functional[5] were used for all computations. A plane wave cutoff energy was set to 400 eV and DFT-D3 method[6] was adopted for the van der Waals correction. In addition, a vacuum space of 15 Å along the z direction was set for catalyst layer to ensure sufficient vacuum and eliminate the periodic interference in the presence of surface adsorption. The convergence thresholds for energy and atomic forces were set as 10^{-5} eV and 0.02 eV/Å, respectively. The optimized catalyst models were frozen and only adsorbates were relaxed in calculations of reaction energy barrier. The thermal and zero-point energy corrections of different intermediates adsorbed on constructed catalysts were calculated at the Γ point. The Gibbs free energy change (ΔG)[7] is simply defined as:

$$\Delta G = \Delta E + \Delta E_{ZPE} - T\Delta S$$

where ΔE is the change of reaction free energy directly obtained from DFT total energies, ΔE_{ZPE} is the change of zero-point energy, T is the temperature (298.15 K), and ΔS is the change in entropy.

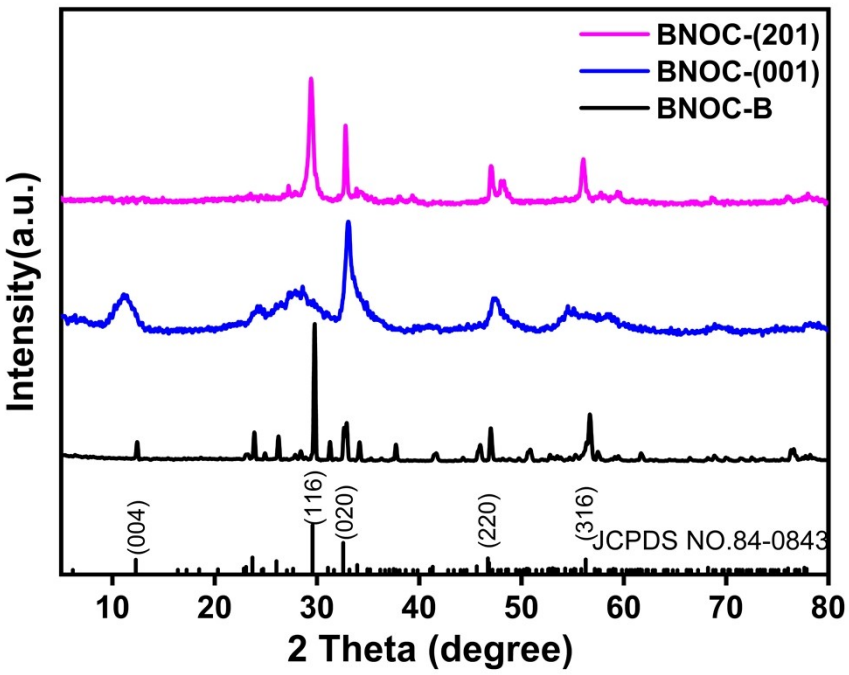

Fig. S1 XRD patterns of BNOC-B, BNOC-(001), and BNOC-(201).

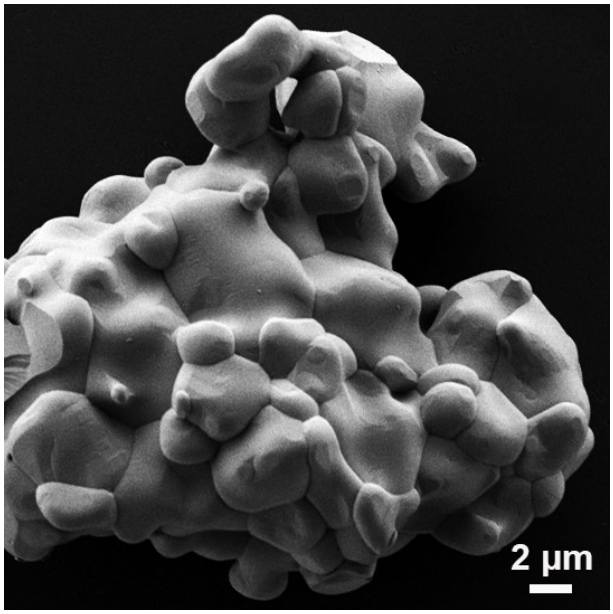

Fig. S2 FE-SEM image of BNOC-B.

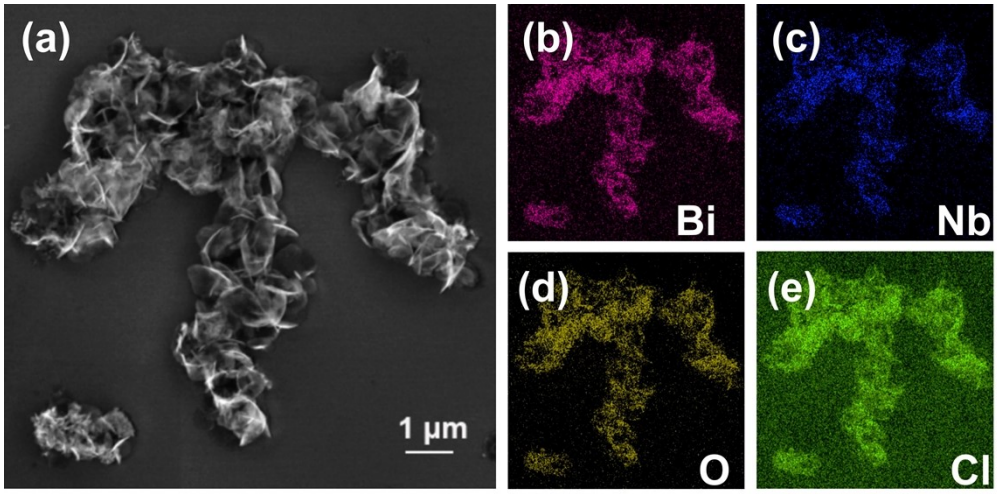

Fig. S3 (a) FE-SEM image and (b)-(e) EDS mapping of BNOC-(201).

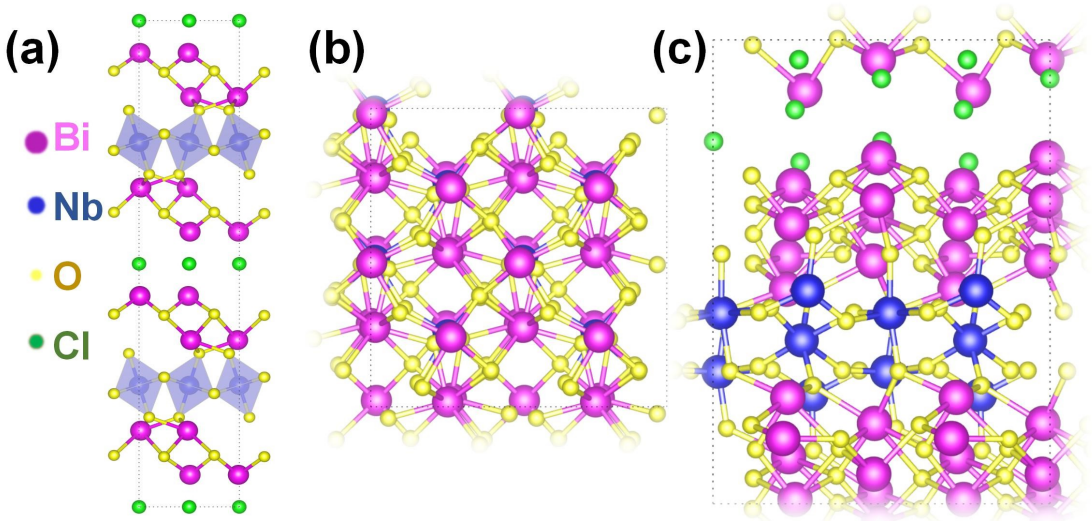

Fig. S4 Crystalline model of (a) BNOC-B, (b) BNOC-(001), and (c) BNOC-(201).

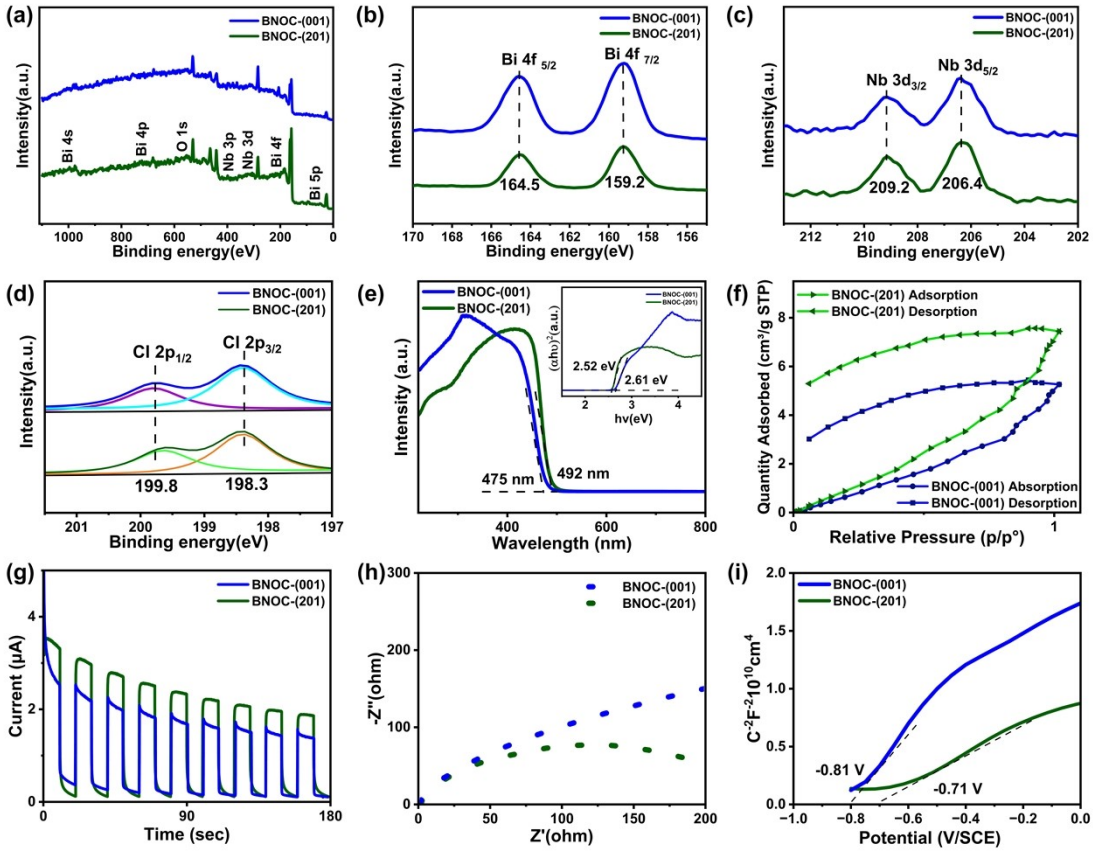

Fig. S5 (a) XPS survey spectra, (b) Bi 4f, (c) Nb 3d, (d) Cl 2p. (e) UV-visible absorption spectrum (inset:the corresponding band edge). (f) CO_2 adsorption and desorption isotherms. (g) Transient photocurrent responses(it), (h) Electrochemical impedance spectra (EIS), (i) Mott-Schottky(M-S) of BNOC-(001) and BNOC-(201).

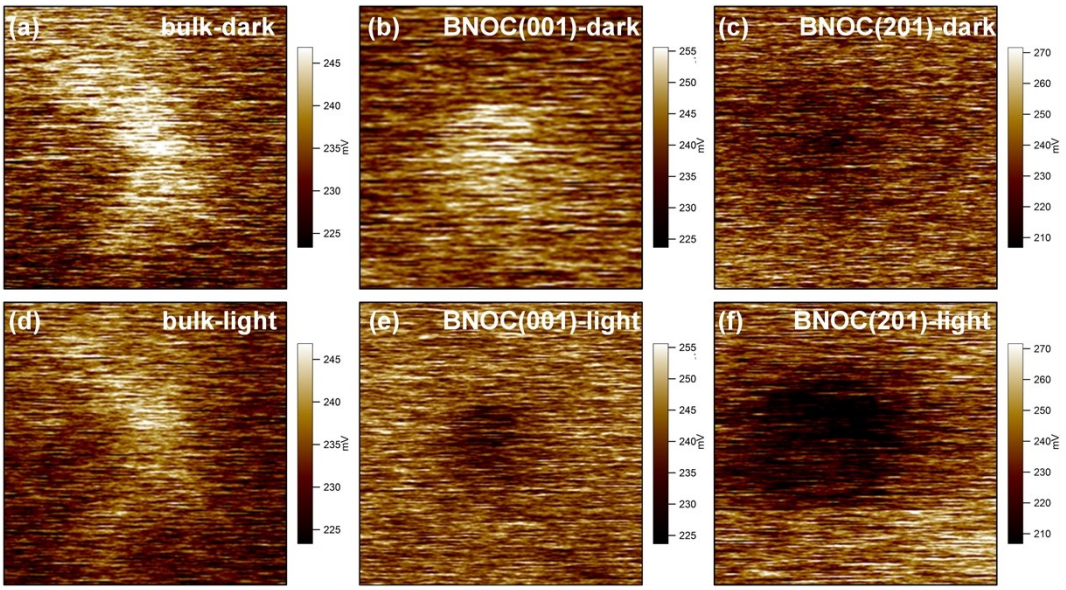

Fig. S6 Surface potential images of BNOC-B (a) before and (d) after light illumination, surface potential images of BNOC-(001) (b) before and (e) after light illumination, surface potential images of BNOC-(201) (c) before and (f) after light illumination.

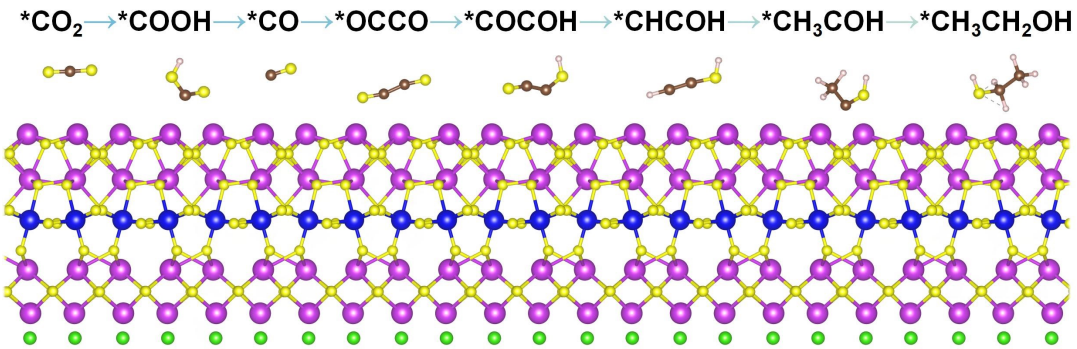

Fig. S7 Schematic pathways of C_2H_5OH hydrocarbon formation on BNOC-(001).

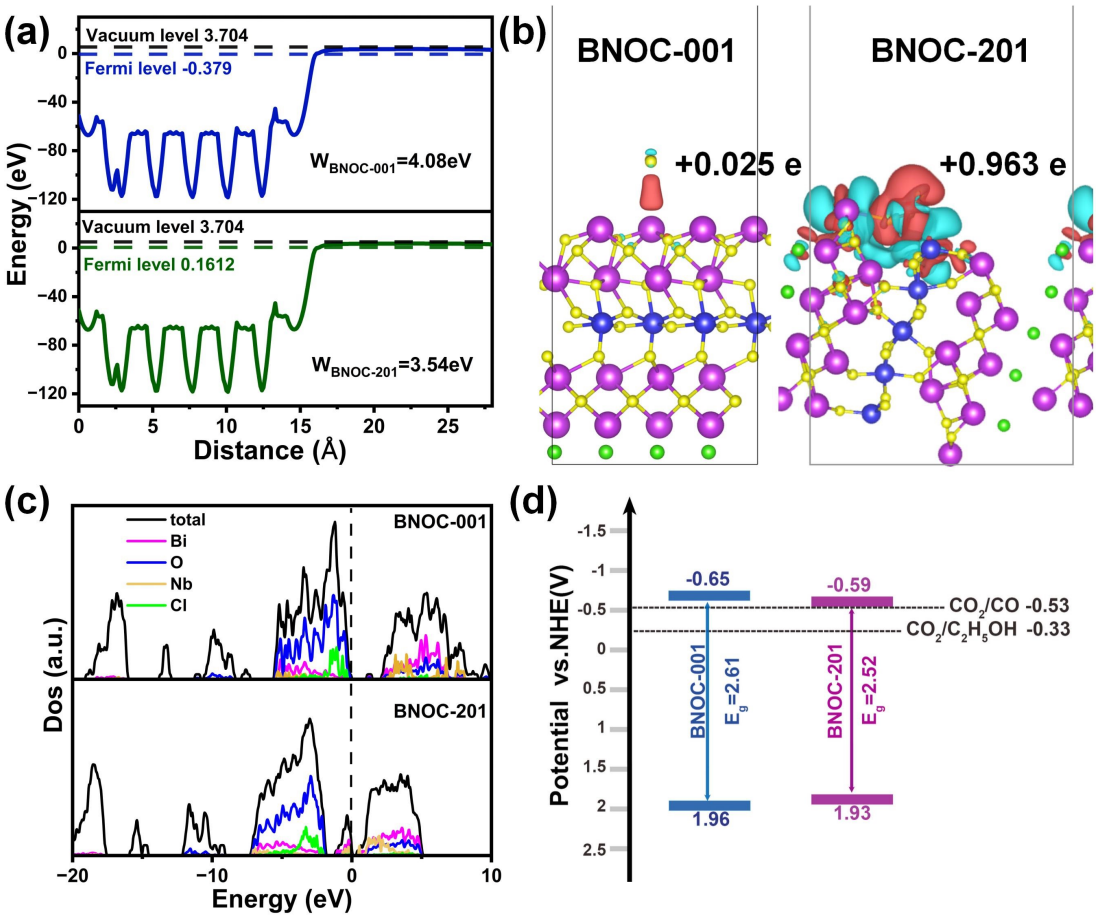

Fig. S8 Calculated (a) electrostatic potentials, (b) charge density differences of *CO_2 (Brown represents electron accumulation, cyan represents electron depletion), (c) TDOS and PDOS projected onto each constituent element, (d) band alignments of BNOC-(001) and BNOC-(201).

$$* CO_2 + H^+ + e^- = *COOH \quad (1)$$

$$* COOH + H^+ + e^- = *CO + H_2O \quad (2)$$

$$* CO \rightarrow CO\uparrow \quad (3)$$

$$* CO + *CO = *OCCO \quad (4)$$

$$* OCCO + H^+ + e^- = *COCOH \quad (5)$$

$$* COCOH + 3H^+ + 3e^- = *CHCOH + H_2O \quad (6)$$

$$* CHCOH + H^+ + e^- = *CH_2COH \quad (7)$$

$$* CH_2COH + H^+ + e^- = *CH_2CHOH \quad (8)$$

$$* CH_2CHOH + H^+ + e^- = *CH_3CHOH \quad (9)$$

$$* CH_3CHOH + H^+ + e^- = *CH_3CH_2OH \quad (10)$$

$$* CH_3CHOH \rightarrow CH_3CH_2OH\uparrow \quad (11)$$

Fig. S9 Pathway of CO_2 photoreduction toward CO and C_2H_5OH on the BNOC.

Supplementary References

1 G. Kresse and J. Furthmüller, *Comput. Mater. Sci.*, 1996, **6**, 15-50.

2 G. Kresse and J. Furthmuller, *Phys. Rev. B*, 1996, **54**, 11169-11186.

3 P. E. Blöchl, *Phys. Rev. B*, 1994, **50**, 17953-17979.

4 G. Kresse and D. Joubert, *Phys. Rev. B*, 1999, **59**, 1758-1775.

5 J. P. Perdew, K. Burke and M. Ernzerhof, *Phys. Rev. Lett.*, 1996, **77**, 3865-3868.

6 S. Grimme, S. Ehrlich and L. Goerigk, *J. Comput. Chem.*, 2011, **32**, 1456-1465.

7 J. K. Nørskov, J. Rossmeisl, A. Logadottir, L. Lindqvist, J. R. Kitchin, T. Bligaard and H. Jónsson, *J. Phys. Chem. B*, 2004, **108**, 17886-17892.